Ice Cloud Absorption Behavior in the Thermal Infrared Inferred from Laboratory Extinction Measurements

D. L. Mitchell, W. P. Arnott, C. Schmitt, and D. Lowenthal
Desert Research Institute
Reno, Nevada

J. M. Edwards
Hadley Centre for Climate Prediction and Research
Meteorological Office
Bracknell, United Kingdom

Introduction

Ice particle-radiation interactions differ from cloud droplet-radiation interactions due to differences in 1) phase functions and 2) the relationship between area and mass, the latter affecting shortwave albedo and longwave emissivity via changes in optical depth (for a given ice water path). However, there is possibly yet a third way by which atmospheric ice- and water-radiation interactions differ: photon tunneling effects (e.g., Nussenzveig 1977; Guimaraes and Nussenzveig 1992). The absence of tunneling effects in ice crystals would reduce their absorption cross section (and the absorption efficiency) in the thermal infrared (IR) by typically 20%, as shown in Figure 1, although in the far IR this reduction (relative to tunneling predicted by Mie theory) can be up to 43% (Mitchell 1998). Hence, IR remote sensing is plagued with large uncertainties until the role of tunneling in ice is resolved.

In an instantaneous flux calculation using the Hadley Centre's Unified Model (HADM4) with a new ice cloud radiation scheme (Mitchell 1998), tunneling effects were most pronounced over the tropics, trapping up to an additional 7 W m^{-2} of outgoing longwave (LW) radiation (OLR), although 3 W m^{-2} was more typical. Globally averaged, it was 1.13 W m^{-2}. The zonally averaged LW heating rate contribution from tunneling in cirrus over the equator was about 0.1 K/day. This is relative to calculations where tunneling effects were removed, and where 100% tunneling corresponds to that predicted by Mie theory for "photon path equivalent spheres."

Tunneling can be viewed as a process by which grazing tangential photons beyond the particle's physical cross section can manifest as surface waves on the particle, and then scatter, or can enter the particle to be absorbed or scattered. This is described in detail in Mitchell (1999), and is illustrated in Figure 2. While it appears plausible for photons beyond the physical cross section to enter into an ice crystal, it also appears possible that, due to the complex geometry of natural ice crystals, such photons may spend less time "orbiting" within a crystal relative to spheres. This would decrease the absorption contribution to tunneling.

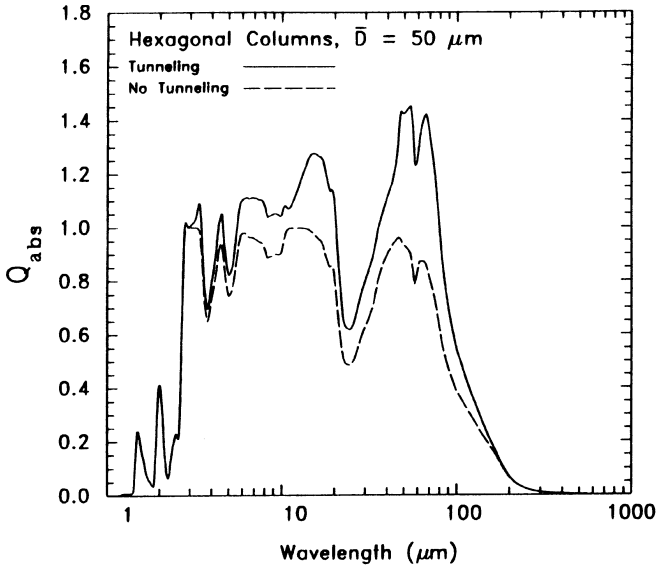

Figure 1. Example of tunneling contributions (100% to absorption efficiency, for an ice size distribution with mean length = 50 μm. Tunneling effects vanish in the Rayleigh regime and when wavelength << D_{eff}.

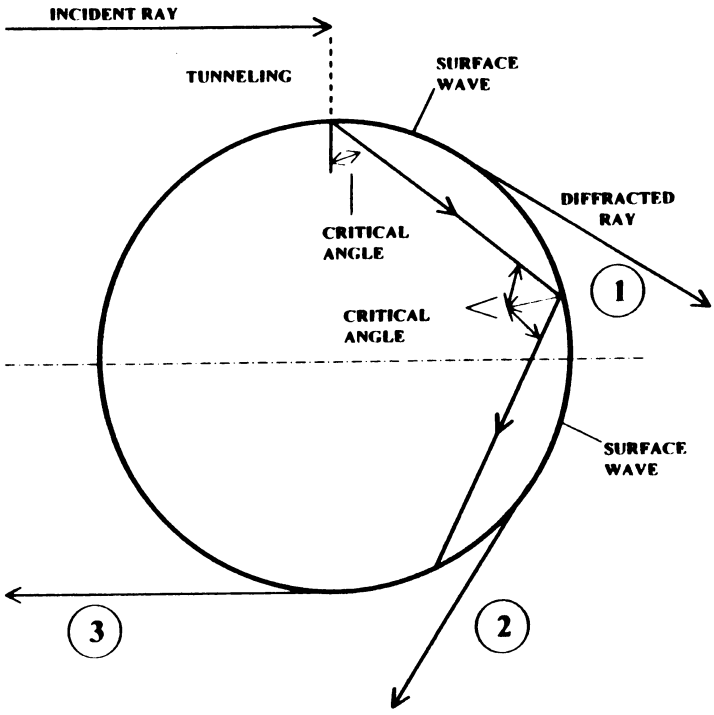

Figure 2. Depiction of possible trajectories of an incident grazing ray after tunneling to the sphere surface. Edge effects are illustrated by ray (1), while rays (2) and (3) are examples of large angle diffraction whereby the ray travels through the sphere and may be absorbed.

FTIR Extinction Measurements

Tunneling is most pronounced when the wavelength within the particle and the particle's effective photon path are similar (Mitchell 1998, 1999). A laboratory experiment was conducted whereby tunneling was investigated using a Fourier Transform Infrared Spectrometer (FTIR) exhibiting a wavelength range of 2 μm to 18 μm, with ice crystals < 50 μm maximum dimension, D. Size distributions exhibited a mean D of about 4 μm to 10 μm. Defining effective diameter (D_{eff}) as

$$D_{ef} = 3/2\,(V_t/P_t) \tag{1}$$

where V_t and P_t = distribution volume and projected area, with V_t referenced to the density of bulk ice (0.92 g cm^{-3}), D_{eff} ranged from about 3.5 μm to 8.2 μm.

The basic experimental design is a modified version of that described in Arnott et al. (1995), where a laser at 0.685 μm penetrates a cloud chamber ice cloud over the same path as the FTIR beam. Ideally, the ice crystals would be large enough such that the extinction efficiency for the laser ($Q_{ext,l}$) equals 2.00. From the FTIR optical depth (τ) and the laser optical depth (τ_l), the IR Q_{ext} is calculated as

$$Q_{ext} = Q_{ext,\,l}\,(\tau/\tau_1) \tag{2}$$

Since Q_{ext} for these crystal sizes will vary as a function of tunneling (up to about 20%), Q_{ext} can be used to estimate the amount of tunneling exhibited by ice crystals. An example is given in Figure 3, showing predicted Q_{ext} for tunneling and no tunneling over the wavenumber range of this experiment, based on hexagonal plates and the Forward Scattering Spectrometer Probe (FSSP) size distribution for run 18 (see Figure 4).

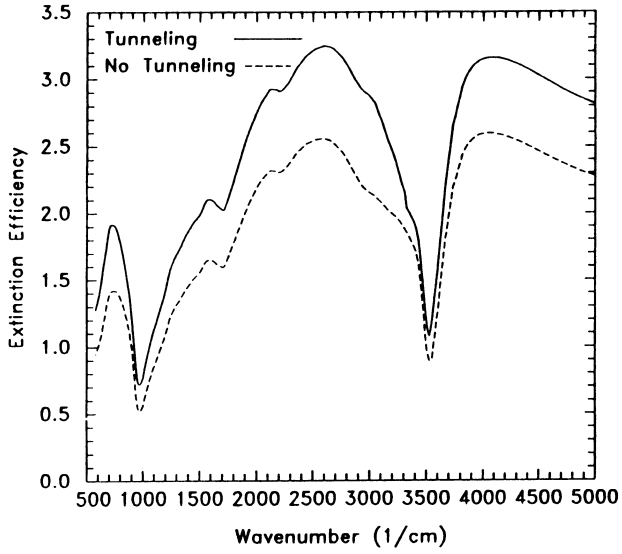

Figure 3. Predicted Q_{ext} values with and without tunneling, based on hex. - plates, the FSSP spectra, and m_f of run 18.

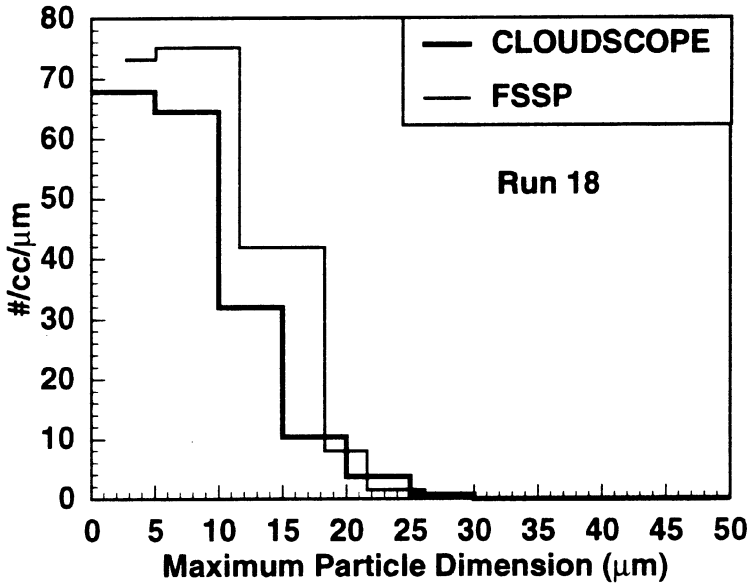

Figure 4. A representative example comparison of size spectra measured by the Cloudscope and FSSP.

To compare this measured Q_{ext} with those predicted, size distributions were measured in the cloud chamber about 30 cm above the FTIR using two instruments: an FSSP and a Cloudscope (CS) (Arnott et al. 1995). Both the CS and FSSP measure D down to about 3 μm. The CS's operating principle is impaction, and concentrations were corrected for changes in collection efficiency. Size spectra from these instruments were similar, as shown in Figure 4, giving confidence that the spectra were realistic. From both spectra, predicted values of Q_{ext} were obtained. The CS video records the ice crystal shapes, which were hexagonal plates throughout this experiment.

Estimates of tunneling amounts can be obtained from the radiation scheme of Mitchell (1998), whereby ice crystals are converted to equivalent photon path spheres, d_e, as defined by (Eq. 1), where P and V now refer to an individual crystal. In this scheme, the tunneling processes are parameterized, as well as the processes of internal reflection/refraction, while extinction due to geometrical blocking, diffraction, and interference is represented through the anomalous diffraction approximation (ADA). Using ice and water spheres, this scheme agrees with Mie theory within 10% for Q_{ext} for size parameters $x > 1.0$, based on the treatment for single particles. Over a range of wavelengths as in this experiment, the mean error is around 2% to 3%. This should yield tunneling estimates within 5% accuracy given zero error or uncertainty in all other aspects of the experiment. Tunneling was quantified as a "tunneling factor," or t_f, ranging from 0 to 1.0, where 0 and 1.0 correspond to ADA (for Q_{ext}) and Mie theory, respectively.

Estimating the Degree of Tunneling

A program that minimizes errors between measured and predicted Q_{ext} values was created, whereby t_f is varied. The radiation scheme requires knowledge of an ice crystal's mass (=> V) and projected area P, which were estimated from the power laws given in Mitchell et al. (1996) for plates, $D \leq 100$ μm. Since

these mass values were inferred from estimated d_e values, there is every possibility that the actual crystal masses in the cloud chamber were different for a given D than those predicted. Moreover, the length-to-width (i.e., aspect) ratio naturally varies considerably for a given D, causing mass to vary also. For these reasons, a mass factor was defined, m_f, which multiplies the mass predicted by the mass-D power law. In summary, both m_f and t_f were optimized to yield the minimum error between the measurement derived and predicted Q_{ext}. Tunneling and mass factors are reported in Table 1.

The optimization procedure was to first assume a t_f of zero and a m_f of 1.0, optimizing first with respect to mass and second with respect to tunneling. The mass optimization sets the basic "pattern" for Q_{ext} (relative minima and maxima), while tunneling controls the amplitude primarily, as shown in Figure 3. The program returns estimates of m_f and t_f, and was rerun with these new estimates until the input and output m_f and t_f values were identical (i.e., convergence). No analysis was performed for $x < 1$. It was found that the assumption of $Q_{ext,l} = 2.00$ was invalid, due to D_{eff} generally giving $x \approx 23$ (see Table 1). Note that $Q_{ext,l} \approx 2$ for $x \geq 30$. For estimating t_f, it is preferable to have $Q_{ext,l}$ independent of t_f. But since t_f must be the same for both the laser and FTIR, rapid convergence and a stable solution was still obtained provided m_f was constrained to 1.0 when estimating $Q_{ext,l}$ for the m_f optimization only. In the t_f optimization, $Q_{ext,l}$ was calculated from optimized m_f values, and the difference between this $Q_{ext,l}$ and the initial $Q_{ext,l}$ was 1.3% for the FSSP spectra, except run 23 where the difference was 12%. For the CS, these differences were ≤ 11%, averaging 6%. Hence, the FSSP results are considered to have the lowest uncertainties.

Results and Discussion

The primary results of this analysis are given in Table 1. The experimental runs listed were chosen due to good agreement between CS and FSSP size spectra. This is evident upon comparison of D_{eff} obtained from these instruments (Table 1). Absolute mean errors are relative to measurement-derived values of Q_{ext}, where the absolute value of the error is summed over all wavelengths and divided by the number of wavelengths.

An example of how predicted and measurement derived Q_{ext} values compare is given in Figure 5 for run 18. The CS and FSSP produce different $Q_{ext,l}$ values, yielding two sets of measurement-derived Q_{ext} values, but for this run the two sets overlap, appearing as one. No data appears in sections where water vapor and CO_2 absorption contributed to Q_{ext}. For all comparisons, predicted Q_{ext} values gave underestimates at the lowest wavenumbers and overestimates at the higher wavenumbers.

It is somewhat remarkable that m_f values range between 0.8 and 1.8, and are generally close to 1.0, given the variability of natural crystal masses (e.g., Mitchell et al. 1990). These results support the mass-D power law for hexagonal plates, $D < 100$ μm, given in Mitchell et al. (1996). Note that m_f and D_{eff} values generally increase from runs 13-20. This coincides with a period when an ice cloud in the chamber was growing.

Table 1. Optimization factors for ice particle mass and photon tunneling.

Run	Tunneling Factor		Mass Factor		Effective Diameter (microns)		Absolute Mean Factor	
	CS	FSSP	CS	FSSP	CS	FSSP	CS	FSSP
13	0.55	0.55	1.15	1.00	5.22	5.02	9.0	8.2
14	0.55	0.60	1.10	1.00	5.64	4.96	11.3	8.9
15	1.00	0.50	1.00	1.05	5.54	5.12	14.9	8.9
16	0.55	0.35	1.35	1.25	6.14	6.01	10.0	8.2
17	0.35	0.40	1.30	1.35	6.95	6.37	10.5	8.5
18	0.35	0.25	1.40	1.40	6.52	6.64	9.4	8.7
19	0.00	0.20	1.60	1.50	8.30	7.23	11.0	8.4
20	0.10	0.05	1.80	1.65	8.19	8.04	9.3	8.3
21	0.00	0.00	1.70	1.55	8.97	8.21	16.5	15.8
22	0.00	0.05	0.88	1.00	3.59	3.97	19.4	19.2
23	0.00	0.00	0.90	0.82	3.68	3.54	20.3	20.1
24	0.10	0.05	1.15	1.00	5.52	5.43	6.3	9.5
Mean	0.30	0.25	1.28	1.21			12.3	11.1
Means without runs 21-23							10.2	8.6

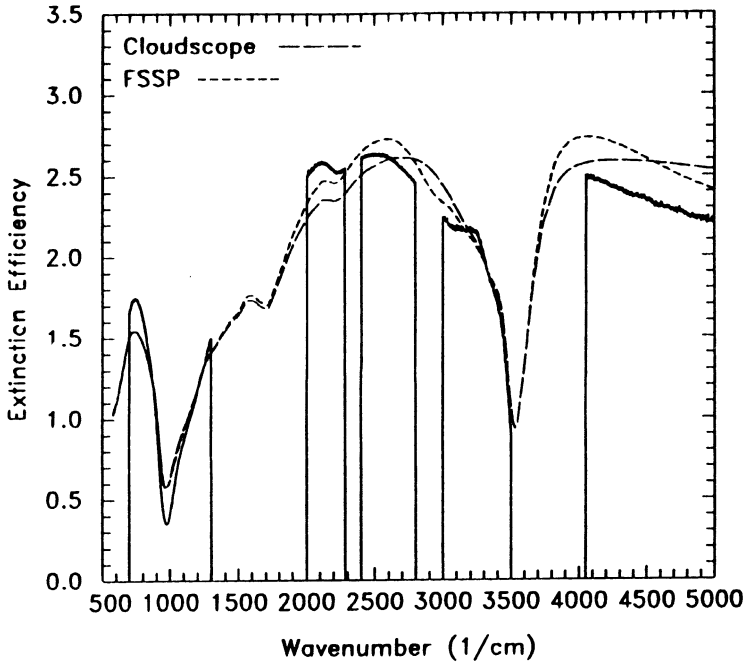

Figure 5. Comparison of measurement-derived Q_{ext} spectra (solid curve) for run 18 with Q_{ext} predicted from the error minimization program, based on CS and FSSP size spectra. Measured values are absent in spectral regions where interference by gases occurred.

This cloud was replaced by a second cloud air mass during runs 22-23, and a third cloud entered the chamber for run 24. Run 21 was during a transition period. Using the retrieval method of Arnott et al. (1997), a size distribution was retrieved from the FTIR spectra of run 21, and was found to be rather dissimilar to the ones measured. Moreover, the cloud chamber is known to exhibit strong temperature inversions, inhibiting mixing. It is possible that the CS and FSSP sampled cloud having different size spectra than were sampled by the FTIR and laser during run 21, possibly explaining the relatively large errors. The larger errors in runs 22-23 appear at least partially due to the smaller crystal sizes present, yielding lower Q_{ext} values as the Rayleigh regime is approached. Hence, seemingly modest errors appear as relatively large percent errors due to the smaller Q_{ext} values.

Noting the above possible exceptions, agreement between predicted and measurement-derived Q_{ext} values appears good, especially for predictions based on the FSSP. The slightly larger errors associated with the CS may be related to the poorer sampling statistics and greater uncertainties associated with $Q_{ext,l}$. This agreement yields some confidence that the tunneling factors in Table 1 are meaningful.

The tunneling factors obtained indicate that for small hexagonal plates, tunneling is not negligible, nor is Mie theory appropriate for treating such crystals. While it should be noted that these results are preliminary, these initial findings suggest tunneling phenomena could be variable, and in general might be 1/4 to 1/3 as strong as tunneling exhibited by spheres, for the small particle mode of size distributions peaking near D = 10 μm.

These results are also consistent with the theoretical T-matrix results in Baran et al. (1998), where it was found that tunneling became negligible for oblate spheroids when the aspect ratio was 6 or higher. During a recent similar experiment, where temperatures varied between -15 °C and -20 °C at the FTIR spectrometer, plate aspect ratios were observed to follow the relationship

$$H = 0.737\ D^{0.6885}\ (\mu m\ units) \qquad (3)$$

where H = plate thickness. At the FTIR level in this current experiment, temperatures were at -10 °C beginning with run 13, and steadily increased to -7.6 °C by run 24. Temperatures aloft were around -15 °C. This suggests that the aspect ratios here may have been lower than predicted by Eq. (3), but were probably not greater. Since the aspect ratios were apparently < 6, some tunneling would be expected based on the Baran et al. work. For D > 100 μm, plate aspect ratios are typically > 6, with the Baran et al. work suggesting negligible tunneling at these larger sizes.

More work is currently under way to evaluate tunneling for hexagonal columns.

Acknowledgments

The Environmental Sciences Division of the U.S. Department of Energy (DOE) funded this work as part of the Atmospheric Radiation Measurement (ARM) Program. The radiation treatment used here is freely available upon request.

References

Arnott, W. P., Y. Dong, and J. Hallett, 1995: Extinction efficiency in the infrared (2-18 μm) of laboratory ice clouds: observations of scattering minima in the Christiansen bands of ice. *Appl. Opt*., **34**, 541-551.

Arnott, W. P., C. Schmitt, Y. Liu, and J. Hallett, 1997: Droplet size spectra and water-vapor concentration of laboratory water clouds: inversion of Fourier transform infrared (500-5000 cm^{-1}) optical-depth measurement. *Appl. Opt*., **36**, 5205-5216.

Baran, A. J., J. S. Foot, and D. L. Mitchell, 1998: The question of ice crystal absorption: A comparison between T-matrix, Mie and anomalous diffraction theory and implications for remote sensing. *Appl. Opt*., **37**, 2207-2215.

Guimaraes, L. G., and H. M. Nussenzveig, 1992: Theory of Mie resonances and the ripple fluctuations. *Optics Commun.*, **89**, 363-369.

Mitchell, D. L., 1999: Parameterization of the Mie extinction and absorption coefficients for water clouds: A process oriented approach. Submitted to *J. Atmos. Sci.*

Mitchell, D. L., 1998: Parameterizing the extinction and absorption coefficients in ice clouds: A process oriented approach. Preprints, Conference on Light Scattering by Nonspherical Particles: Theory, Measurements, and Applications. AMS, September 29-October 1, 1998, New York, 40-43.

Mitchell, D. L., A. Macke, and Y. Liu, 1996: Modeling cirrus clouds. Part II: Treatment of radiative properties. *J. Atmos. Sci*., **53**, 2967-2988.

Mitchell, D. L., R. Zhang, and R. L. Pitter, 1990: Mass-dimensional relationships for ice particles and the influence of riming on snowfall rates. *J. Appl. Meteor*., **29**, 153-163.

Nussenzveig, H. M., 1977: The theory of the rainbow. *Sci. Am.*, **236**, 116-127.